# Supplementary Information

## Enhancing the coupling reaction between $CO_2$ and epoxides over amino-functionalized defective-UiO-66

Guoqing He,[a1] Yonghao Liang,[a1] Li Guo,*[a] Qianqian Zhang,[a] Ying Xie,[a] Zefan Hu,[a] Jialing Chen,[a] Xiaoqin Wu*[a] and Ran Zhang,*[b]

[a] Key Laboratory of Hubei Province for Coal Conversion and New Carbon Materials, School of Chemistry and Chemical Engineering, Wuhan University of Science and Technology, Wuhan 430081, China

[b] Hubei Key Laboratory of Biomass Fibers and Eco-dyeing & Finishing, Wuhan Textile University, Wuhan 430073, China.

* Correspondence: guoli@wust.edu.cn (L.G.); wuxiaoqin@wust.edu.cn (X.W.); rzhang@wtu.edu.cn (R.Z.)

[1] These authors contributed equally to this work.

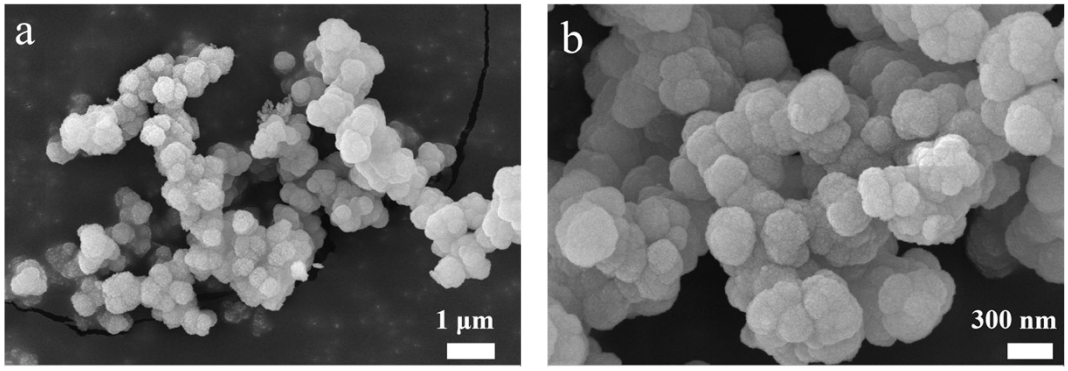


**Fig. S1** SEM images of UiO-66-DABA$_{0.2}$.

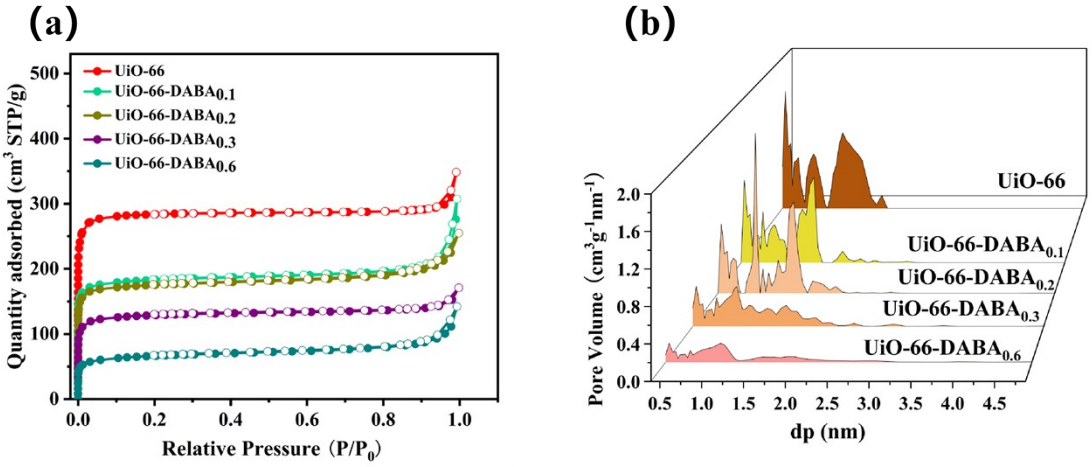


**Fig. S2** (a) The $N_2$ adsorption-desorption isotherms of UiO-66 and UiO-66-DABA$_x$ samples; (b) NLDFT pore size distribution of UiO-66-DABA$_x$.

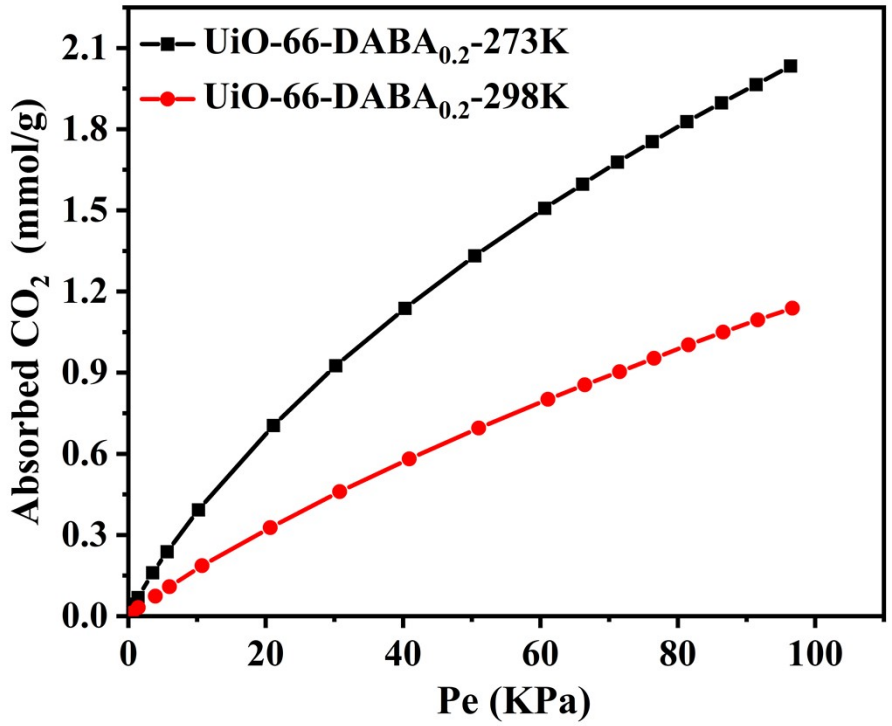


**Fig. S3** $CO_2$ adsorption plots of UiO-66-$DABA_x$ samples at 273 K and 298 K.

Taking UiO-66-$DABA_{0.2}$ as a model adsorbent, the volumetric adsorption capacities measured experimentally were first converted to molar adsorption capacities via Formula (1). Subsequently, by identifying the pressures corresponding to an identical adsorption capacity at various temperatures from Fig. S1, the isosteric heat of adsorption ($Q_{st}$) was calculated using Formula (2).

$$P_e \cdot V_a /(RT) = n \tag{1}$$

$$(T_2 - T_1)Q_{st} /(RT_1T_2) = \ln(P_2 / P_1) \tag{2}$$

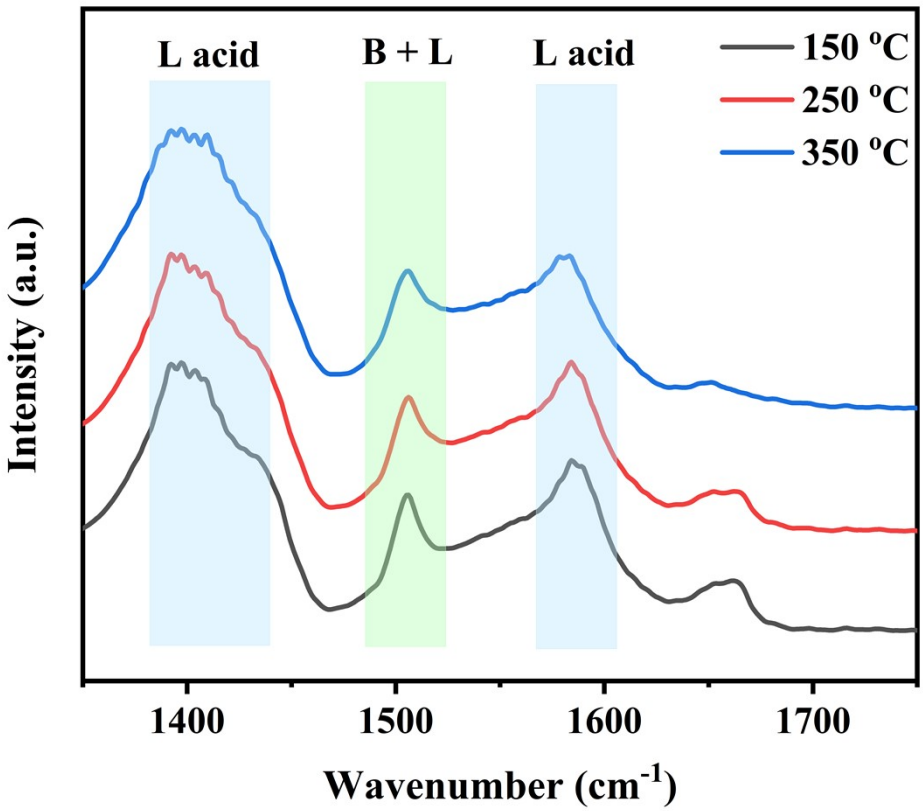


**Fig. S4** Py-IR data of UiO-66-DABA$_{0.2}$.

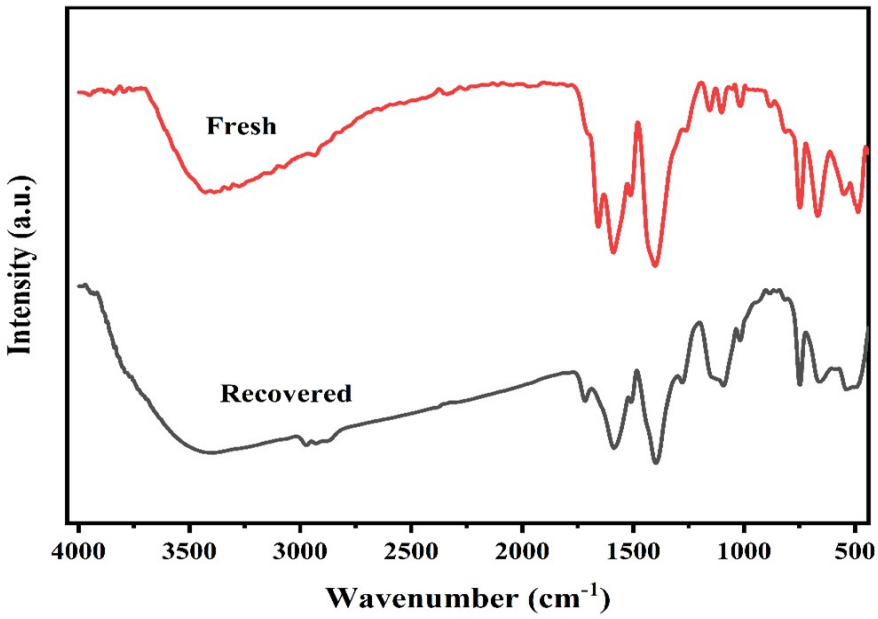


**Fig. S5** FTIR spectra of fresh UiO-66-DABA$_{0.2}$ and UiO-66-DABA$_{0.2}$ after reaction.

In Fig. S5, the peak in the range of 1500-1660 cm$^{-1}$ belonged to C=O in the carboxylate. The peak in the range of 1450-1500 cm$^{-1}$ was ascribed to the aromatic C=C of the organic linker. Meanwhile, the peak in the range of 1250-1450 cm$^{-1}$ was attributed to the stretching vibration of -COOH in the UiO-66-DABA$_{0.2}$. Furthermore, the peak in the range of 2900-3500 cm$^{-1}$ can be ascribed to stretching vibration peak of -OH, -$NH_2$, and -$CH_2$ in the UiO-66-DABA$_{0.2}$. Comparison of the FTIR spectra of the catalyst before and after the reaction revealed no obvious changes, suggesting that the primary functional groups of the catalyst were well preserved during the reaction.

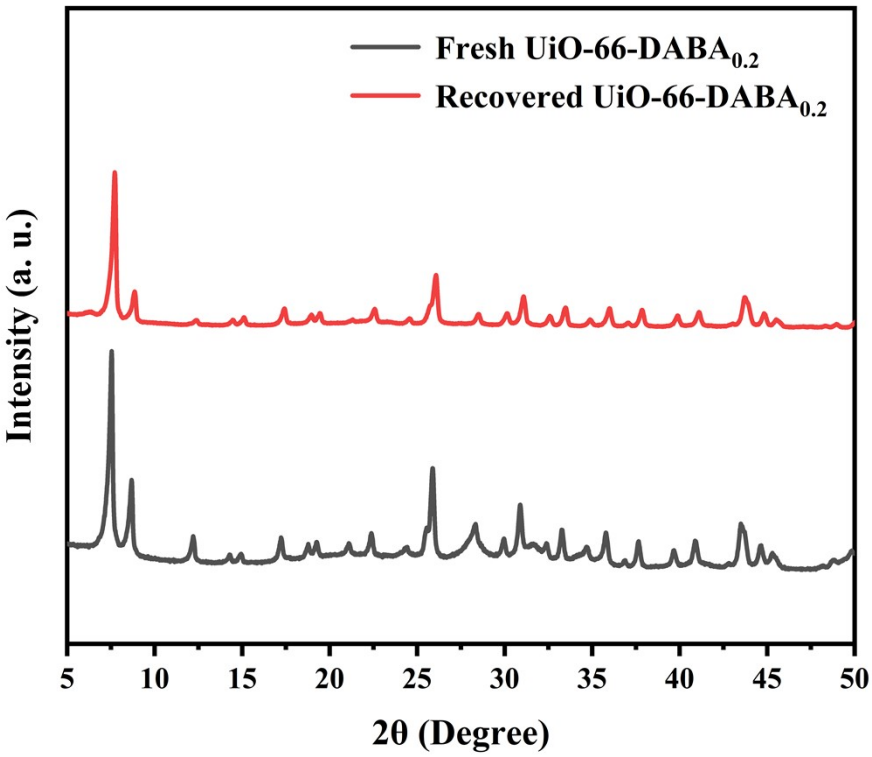


**Fig. S6** XRD patterns of fresh UiO-66-DABA$_{0.2}$ and UiO-66-DABA$_{0.2}$ after reaction.

Subsequently, the XRD patterns of UiO-66-DABA$_{0.2}$ before and after the reaction were carefully studied (Fig. S6). No significant changes were observed in the characteristic diffraction peaks of UiO-66-DABA$_{0.2}$ at 7.57°, 8.66°, and 25.87° before and after the reaction.

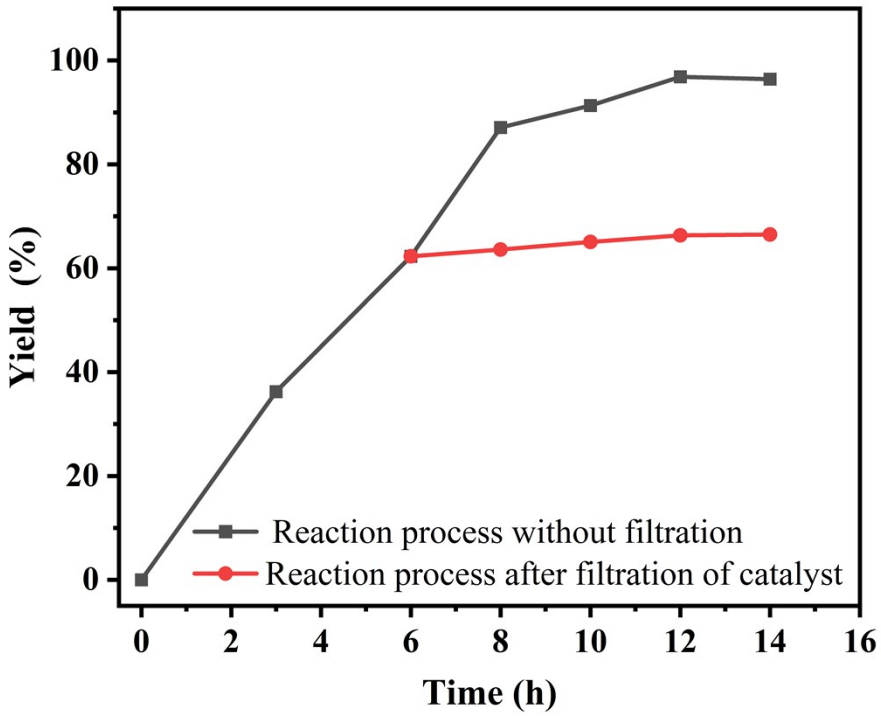


**Fig. S7** Leaching test (hot filtration test) for the UiO-66-DABA$_{0.2}$ catalyzed cyclic carbonates formation. Reaction conditions: Reaction conditions: epoxycyclohydrin (20 mmol), UiO-66-DABA$_{0.2}$ (0.1 g), co-catalyst (KBr, 1.0 mol% of epoxide), $CO_2$ 1.0 MPa, 90 °C.

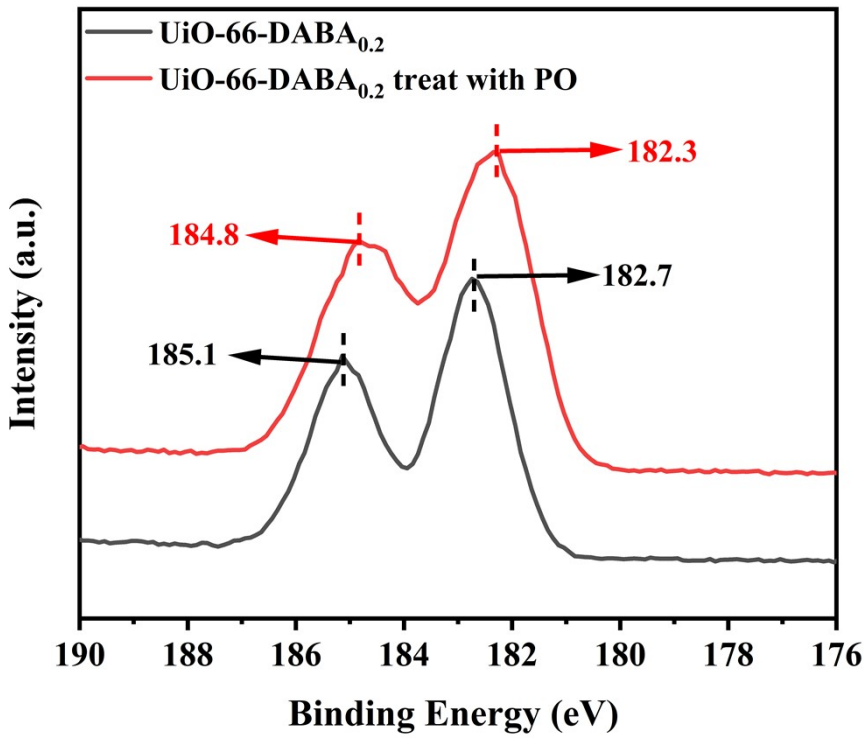


**Fig. S8** Zr 3d of UiO-66-DABA$_{0.2}$ before and after treat with PO.

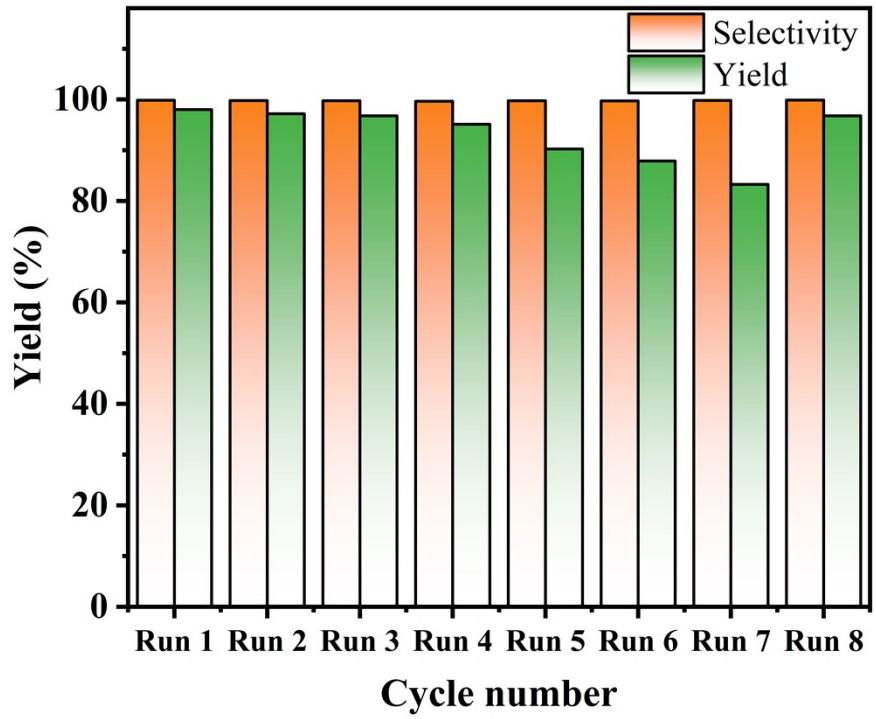


**Fig. S9** Recycling performance of the UiO-66-$DABA_{0.2}$ catalyst. Standard conditions: propylene oxide (20 mmol), UiO-66-$DABA_x$ (0.1 g), co-catalyst (0.2 mmol), $CO_2$ pressure (1 MPa), 90 °C, and 12 h.

During the first seven catalytic cycles, a mechanical loss of 5-8 mg per cycle occurred due to washing and filtration procedures. In the 8th cycle, the catalyst loading was re-supplemented to the initial amount used in the fresh reaction, and the catalytic activity was fully restored. These results indicate that the gradual decline in activity during recycling is primarily attributed to physical/mechanical loss of the catalyst rather than intrinsic deactivation.

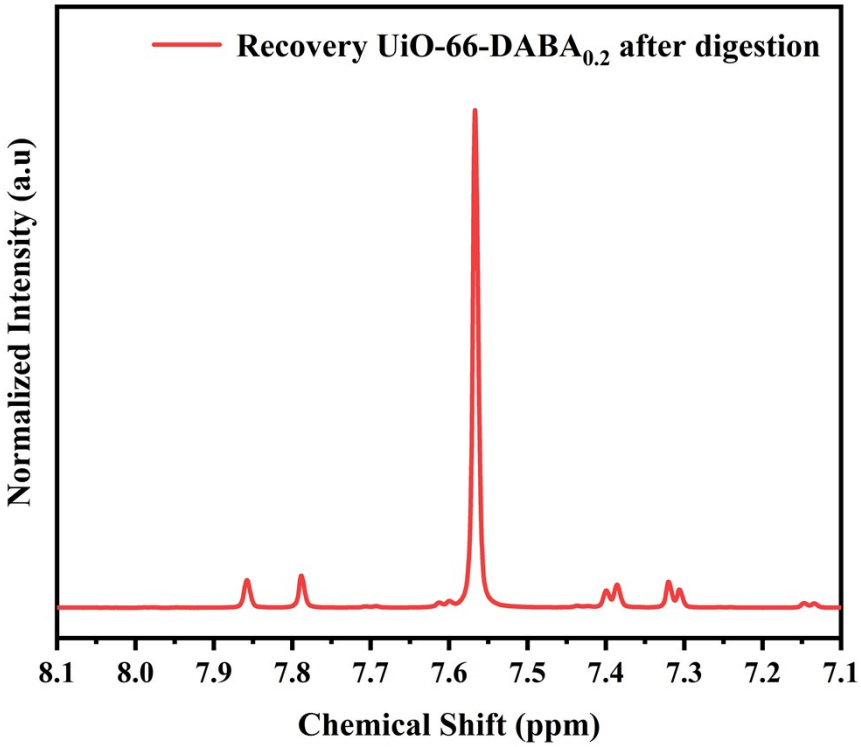


**Fig. S10** $^{1}$H NMR spectra of UiO-66-DABA$_{0.2}$ after digestion.

The dissolution/$^{1}$H NMR spectra obtained on the recovery UiO-66-DABA$_{0.2}$ after reaction were shown in Fig. S10, where it could be seen that mixed ligands (BDC and DABA). $^{1}$H NMR results revealed no obvious changes in the species and content of the ligand before and after the reaction, which is consistent with the FTIR and XRD characterization results. This confirms that the structure of the catalyst remained essentially unchanged during the reaction.

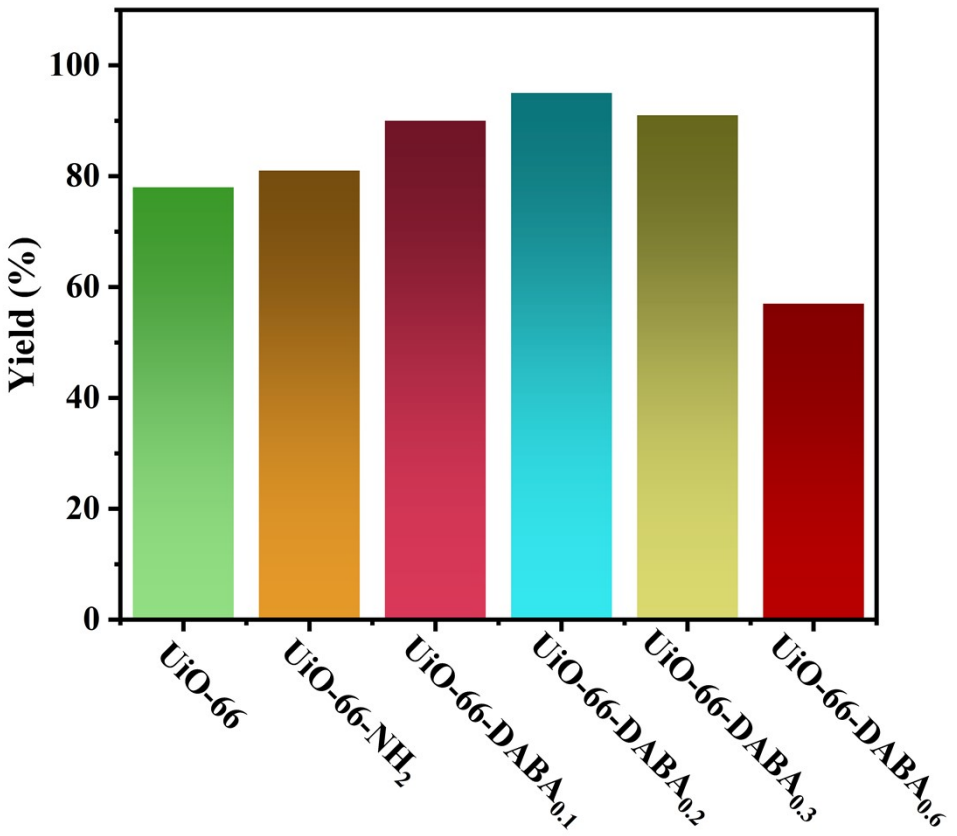


**Fig. S11** Comparison of the catalytic activity of UiO-66-based catalyst. Reaction conditions: propylene oxide (20 mmol), UiO-66-DABA$_x$ (0.1 g), co-catalyst (0.2 mmol), $CO_2$ pressure (1 MPa), 90 $^oC$, and 12 h.

To distinguish the individual contributions of Lewis acidic $Zr^{4+}$ sites and basic -$NH_2$ groups, we designed a series of control catalysts with isolated functionalities, and their catalytic performances were systematically evaluated. Pristine UiO-66 (no defects, no -$NH_2$) showed a slightly inferior yield relative to UiO-66-$NH_2$ (no defects, with -$NH_2$), which arises from the absence of basic -$NH_2$ groups (Fig. S11). Defective UiO-66-DABA$_{0.2}$ (with both defects and -$NH_2$) afforded the highest yield of cyclic carbonates (95%), conforming that undercoordinated $Zr^{4+}$ sites dominate epoxide activation and ring opening. Notably, overloading DABA triggers a significant loss of catalytic activity . This deterioration stems from the disruption of the MOF framework (Table S2), thereby hindering substrate adsorption and activation.

Although direct in situ or operando spectroscopic evidence is currently unavailable, the proposed mechanism is strongly supported by indirect evidence from XPS analysis, $CO_2$ adsorption measurements, and control experiments. After

treatment with propylene oxide, the Zr 3d peaks of UiO-66-DABA$_{0.2}$ shift to lower binding energy, confirming electronic interaction between undercoordinated $Zr^{4+}$ sites and epoxide oxygen, which verifies epoxide activation via Lewis acid coordination. Meanwhile, UiO-66-DABA$_{0.2}$ exhibits a higher $CO_2$ adsorption capacity and isosteric heat of adsorption than pristine UiO-66, demonstrating that -$NH_2$ groups enhance $CO_2$ capture and polarization. Combined with control experiments, these results collectively confirm the synergistic effect of $Zr^{4+}$ Lewis acid sites and basic -$NH_2$ groups in promoting $CO_2$ cycloaddition.

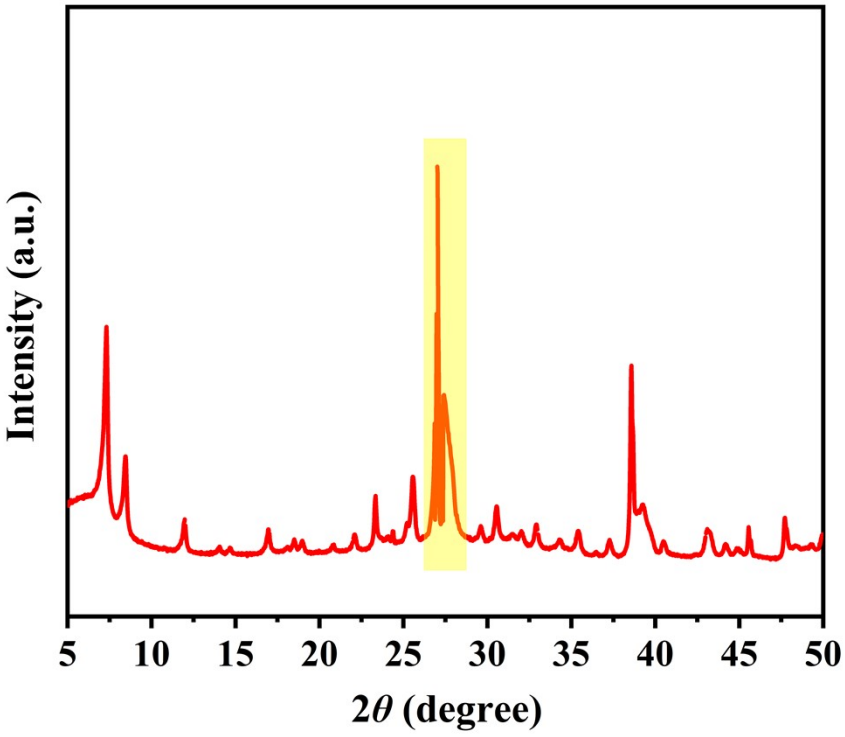


**Fig. S12** XRD patterns of UiO-66-DABA$_{0.2}$ after 8 cycles.

The catalyst maintains the UiO-66 structure within the first four cycles. After eight cycles, both UiO-66 and $ZrO_2$ diffraction peaks are observed, confirming partial crystal structure transformation.

**Table S1.** Adsorption and desorption parameters for UiO-66 and UiO-66-DABA$_x$

| Materials | BET surface | Total pore volume | Micropore volume | Mesopore volume | Micropore volume/Tota |
|---|---|---|---|---|---|

| | area ($m^2g^{-1}$) | ($cm^3g^{-1}$)[a] | ($cm^3g^{-1}$)[b] | ($cm^3g^{-1}$) | l pore volume |
|---|---|---|---|---|---|
| UiO-66 | 1040 | 0.63 | 0.44 | 0.19 | 0.70 |
| UiO-66-$DABA_{0.1}$ | 581 | 0.43 | 0.24 | 0.19 | 0.55 |
| UiO-66-$DABA_{0.2}$ | 557 | 0.38 | 0.22 | 0.16 | 0.58 |
| UiO-66-$DABA_{0.3}$ | 409 | 0.25 | 0.15 | 0.10 | 0.60 |
| UiO-66-$DABA_{0.6}$ | 215 | 0.21 | 0.06 | 0.15 | 0.29 |

[a] The total pore volume determined by use of the adsorption branch of the $N_2$ isotherm at $p/p_0$=0.99.

[b] The specific micropore volume obtained from the *t*-plot.

[c] The mesopore volume is calculated by subtracting micropore volume from the total pore volume.

**Table S2**. Element structure information for UiO-66-$DABA_X$

| Materials | Theory DABA/BDC | $^1$H NMR DABA/BDC | Average of BDC | Number of defects |
|---|---|---|---|---|
| UiO-66 | - | - | 5.9 | 0.1 |
| UiO-66-$DABA_{0.1}$ | 0.11 | 0.09 | 5.0 | 1.0 |
| UiO-66-$DABA_{0.2}$ | 0.25 | 0.23 | 4.6 | 1.4 |
| UiO-66-$DABA_{0.3}$ | 0.43 | 0.34 | 4.2 | 1.8 |
| UiO-66-$DABA_{0.6}$ | 1.50 | 1.21 | 4.1 | 1.9 |

$^1$H NMR spectra were recorded on a Bruker-600 NMR 600 MHz spectrometer; 20 mg powder MOF was dissolved in 1 M 600 μL $NaOH/D_2O$ stock solution. Then, the solution was sonicated for 30 minutes and held at room temperature for 24 hours. This alkaline digestion procedure selectively dissolves the organic components of the framework, including the organic linkers and pore-occluded solvent, whereas the inorganic Zr-containing species precipitate as $ZrO_2$ and settle at the bottom of the tube,

thus remaining undetected in the subsequent NMR analysis.

Accordingly, determining the molar ratio between different species necessitates normalization, in which each integral is divided by the number of equivalent nuclei giving rise to the corresponding signal. A general equation for the molar ratio between two molecules (*Molecule* 1 and *Molecule* 2) can thus be expressed as follows:

$$\frac{Molecule\ 1}{Molecule\ 2}Xi = \left(\frac{Molecule\ 1\ Int.}{Number\ of\ H\ in\ Molecule\ 1}\right) / \left(\frac{Molecule\ 2\ Int.}{Number\ of\ H\ in\ Molecule\ 2}\right)$$

Where,

$\frac{Molecule\ 1}{Molecule\ 2}Xi$ is the molar ratio between *Molecule* 1 and *Molecule* 2.

*Molecule* 1 *Int*. And *Molecule* 2 *Int*. are the numerical values of the integrals obtained on the *Molecule* 1 and *Molecule* 2 $^1$H NMR signals.

*Number of H in Molecule 1* and *Number of H in Molecule 2* are the number of equivalent protons contributing to the respective $^1$H NMR signals of *Molecule* 1 and *Molecule* 2 per molecule.

In order to evaluate the degree of defects in MOF samples, we quantitatively analyzed the TGA data obtained from MOFs.[1] Assuming the ideal (defect free) zirconium cluster of UiO-66 is $Zr_6O_6(BDC)_6$, the residue after complete combustion in thermogravimetric experiments is pure $ZrO_2$, and the reaction formula is as follows:

$$Zr_6O_6(BDC)_6(s) + 45O_2(g) \rightarrow 6ZrO_6(s) + 48CO_2(g) + 12H_2O(g)$$

The molar mass of $Zr_6O_6(BDC)_6$ (1628.03 g mol$^{-1}$) is 2.202 times higher than the molar mass of residual $ZrO_2$ (6 × 123.22=739.34 g mol$^{-1}$). If the weight of TGA running terminals on UiO-66 is normalized to 100%, the ideal position of UiO-66 on the TGA map should be 220.2% ($W_{Ideal.\ Plat.}$). However, it is usually significantly less than this theoretical weight, which means that the UiO-66 framework is lighter than the framework developed in the idealization equation, i.e. the UiO-66 framework may be subject to ligand defects.[2] $Zr_6$ MOF composition can be calculated with the following equation:

$$W_{Ideal.Plat.} = (\frac{M_{Comp.}}{M_{6ZrO_2}}) * W_{End} \quad (3)$$

Where: $M_{Comp.}$ is the molar mass of the composition of the ideal Zr cluster (1628.03 g $mol^{-1}$); $M_{6\,ZrO2}$ is the molar mass of 6 moles of zirconium oxide (739.34 g $mol^{-1}$); $W_{End}$ is the end weight of the TGA run (100 % if normalized as described above).

When quantifying the number of ligand defects (per $Zr_6$ formula unit) in defective UiO-66 samples by this method, the zirconium clusters are present in the form of $Zr_6O_{6+x}(BDC)_{6-x}$, where X is the number of connector defects per $Zr_6$ single formula. The weight of each BDC linker (Wt. $PL_{Theo.}$) can be calculated from formula (4):

$$Wt.PL_{Theo.} = \frac{W_{Ideal.Plat.} - W_{End}}{6} = \frac{220.2 - 100}{6} = 20.03\% \quad (4)$$

The actual number of connectors ($N_{Exp.}$) (6-x in $Zr_6O_{6+x}(BDC)_{6-x}$) for each defective $Zr_6$ type unit can be calculated by formula (5), in which the idealized numerical $W_{Ideal.\ Plat.}$. replace with the actual numeric value $W_{Exp.\ Plat}$. That is, the number X of connector defects in each $Zr_6$ formula unit can be calculated from formula (6):

$$N_{Exp.} = (6 - x) = \frac{(W_{Exp.Plat.} - W_{End})}{Wt.PL_{Theo.}} \quad (5)$$

$$x = 6 - N_{Exp.} = 6 - (\frac{W_{Exp.Plat.} - W_{End}}{Wt.PL_{Theo.}}) \quad (6)$$

**Table S3** The cycloaddition reaction of UiO-66-DABA$_{0.2}$ with different epoxides[a]

| Entry | Epoxide | Product | Selectivity (%)[c] | Yield (%) |
|---|---|---|---|---|
| 1 |  | 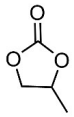 | 99 | 95 |
| 2 | 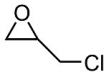 | 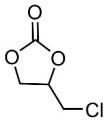 | 99 | 97 |
| 3 | 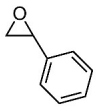 | 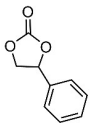 | 98 | 86 |
| 4 |  | 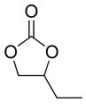 | 99 | 92 |
| 5[b] | 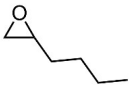 | 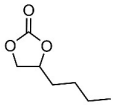 | 97 | 87 |
| 6 | 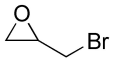 | 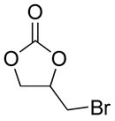 | 97 | 90 |
| 7[b] |  | 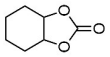 | 98 | 46 |

[a] Reaction conditions: epoxide (20 mmol), UiO-66-DABA$_{0.2}$ (0.1 g), co-catalyst (KBr, 1.0 mol% of epoxide), $CO_2$ 1.0 MPa, 90 °C, 12 h.

[b] Reaction conditions: epoxide (20 mmol), UiO-66-DABA$_{0.2}$ (0.1 g), co-catalyst (KBr, 1.0 mol% of epoxide), $CO_2$ 1.0 MPa, 120 °C, 12 h.

[c] Determined by GC and GC-MS.

**Table S4**. Zr contnet of UiO-66-DABA$_{0.2}$ before and after reaction

| Entry | Catalyst | Zr contents (wt%)[a] |
|---|---|---|
| 1 | Fresh UiO-66-DABA$_{0.2}$ | 53.67 |
| 2 | Recovered UiO-66-DABA$_{0.2}$ | 51.28 |

[a] Zr contents were analyzed by ICP-OES.

**Table S5**. The activation energy required for cycloaddition of different catalysts

| Entry | Catalyst system | Catalytic substrate | Activation Energy (kJ/mol) | Ref. |
|---|---|---|---|---|
| 1 | Iron complexes /TBAB | PO | 98.4 | 3 |
| 2 | [HMIM]Br | PO | 62.6 | 4 |
| 3 | $NH_3Br$/Al-SBA-15 | PO | 51.3 | 5 |
| 4 | Mim/$ZnBr_2$ | PO | 41.1 | 6 |
| 5 | HIL@Cr-MIL-101 | PO | 55.3 | 7 |
| 6 | UiO-66-$DABA_{0.2}$ | PO | 37.2 | this work |

**Table S6**. Catalytic Performance of MOF-Based and Non-MOF Systems for the Synthesis of Cyclic Carbonates

| Entry | Catalyst system | Substrate (mmol) | Quantity of catalyst (mg) | Yield (%) | TON[a] | TOF[b] | Ref. |
|---|---|---|---|---|---|---|---|
| 1 | UMCM-1-$NH_2$ | 18.6 | 100 | 90 | 141.6 | 5.9 | 8 |
| 2 | Ni@TFPCPa COF(MC) | 5 | 60 | 92 | 23.3 | 0.97 | 9 |
| 3 | polyILs@MIL-101 | 1 | 100 | 94 | 3.1 | 0.06 | 10 |
| 4 | ILA@U6N | 25 | 60 | 93 | 183.1 | 45.8 | 11 |
| 5 | MIL-101-IMBr-6 | 18.6 | 100 | 93 | 95.2 | 28.3 | 12 |
| 6 | UiO-66-$DABA_{0.2}$/KBr | 20 | 100 | 95 | 35.8 | 2.98 | this work |

[a] TON = product (mmol)/catalyst (mmol).

[b] TOF = product (mmol)/catalyst (mmol)/time (h).

**Table S7**. Catalytic cycloaddition reaction of propylene oxide (PO) and $CO_2$ with different co-catalyst[a]

| Entry | Catalyst | Co-catalyst[b] | Yeild (%)[c] | Sel. (%) |
|---|---|---|---|---|
| 1 | UiO-66-DABA$_{0.2}$ | KCl | 65 | 97 |
| 2 | UiO-66-DABA$_{0.2}$ | KBr | 95 | 99 |
| 3 | UiO-66-DABA$_{0.2}$ | KI | 93 | 99 |
| 4 | UiO-66-DABA$_{0.2}$ | $FeCl_3$ | 86 | 99 |
| 5 | UiO-66-DABA$_{0.2}$ | $ZnCl_2$ | 82 | 98 |
| 6 | UiO-66-DABA$_{0.2}$ | TBAC | 80 | 99 |
| 7 | UiO-66-DABA$_{0.2}$ | TBAB | 93 | 99 |

[a] Reaction conditions: propylene oxide (20 mmol), UiO-66-DABA$_x$ (0.1 g), $CO_2$ pressure (1 MPa), 90 $^oC$, and 12 h.

[b] Co-catalyst is 1.0 mol% of propylene oxide.

[c] Determined by GC and GC-MS.

A series of co-catalysts were tested to clarify the contributions of the MOF and halide-assisted pathways (Table S7). UiO-66-DABA$_{0.2}$ alone afforded 68% yield, confirming intrinsic activity from $Zr^{4+}$/-$NH_2$ synergy. KBr delivered the highest yield (95%), followed by KI and TBAB (93%), while KCl and TBAC gave only 65% and 80%. The activity trend $Br^- \approx I^- \gg Cl^-$ reflects nucleophilicity and leaving-group ability. The MOF provides 68% baseline activity, and bromide-assisted ring opening contributes the additional 27% enhancement, highlighting their cooperative role.

**GC-MS results:**

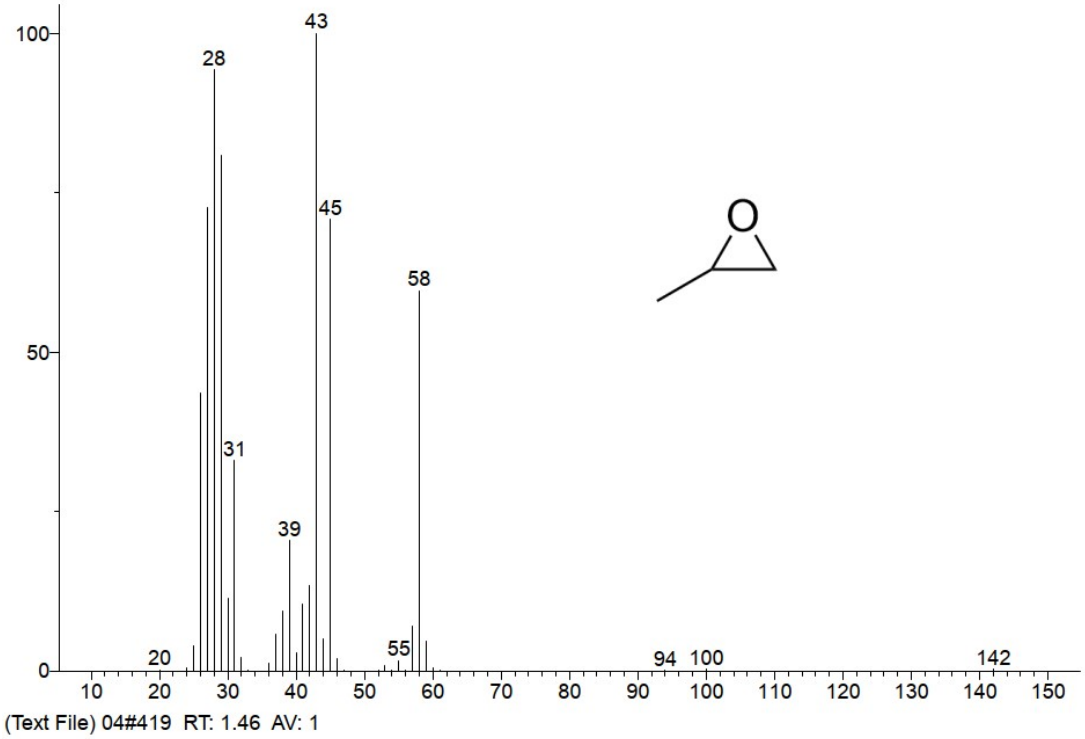

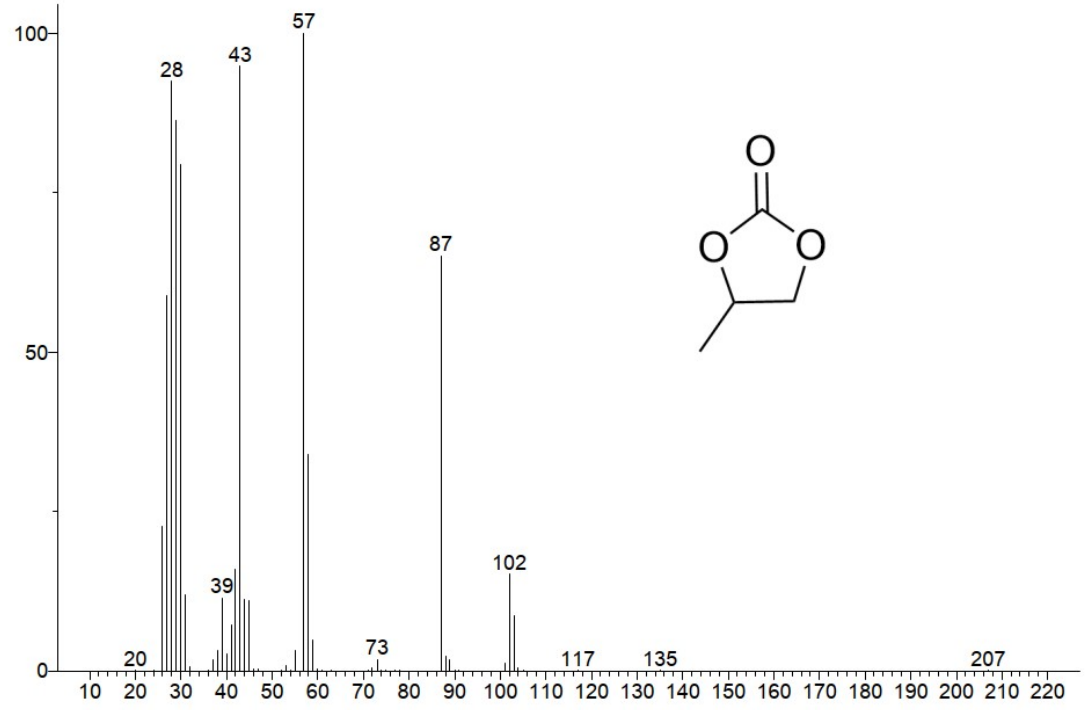


(Text File) 1#1141 RT: 3.95 AV: 1

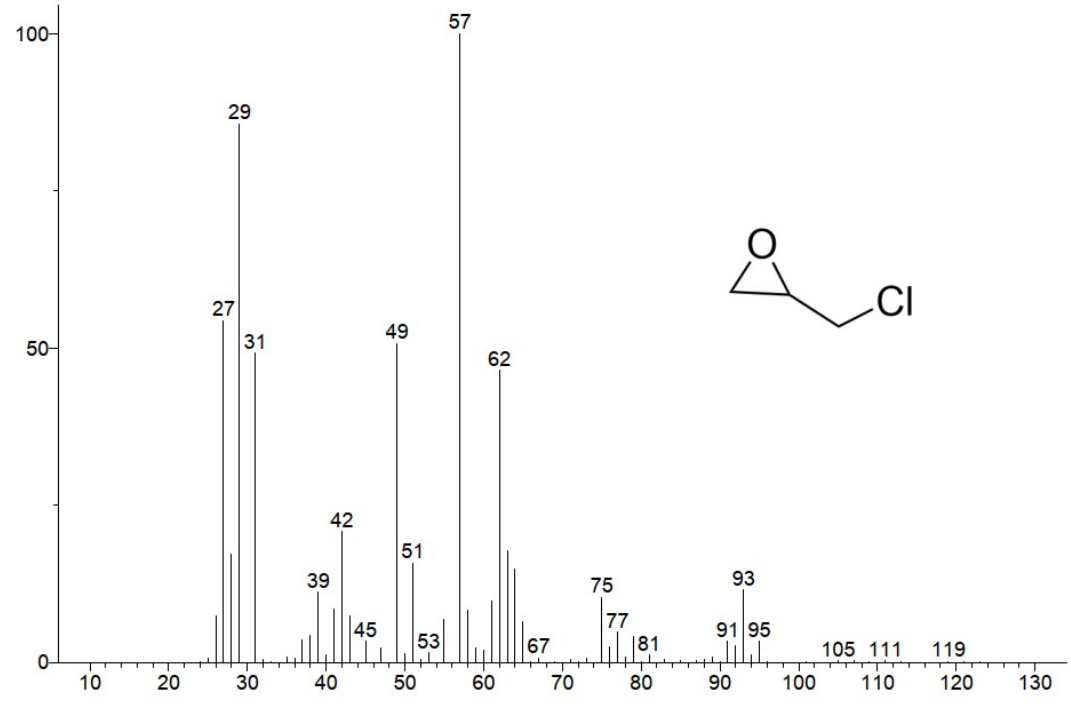


(Text File) data03#424 RT: 1.47 AV: 1

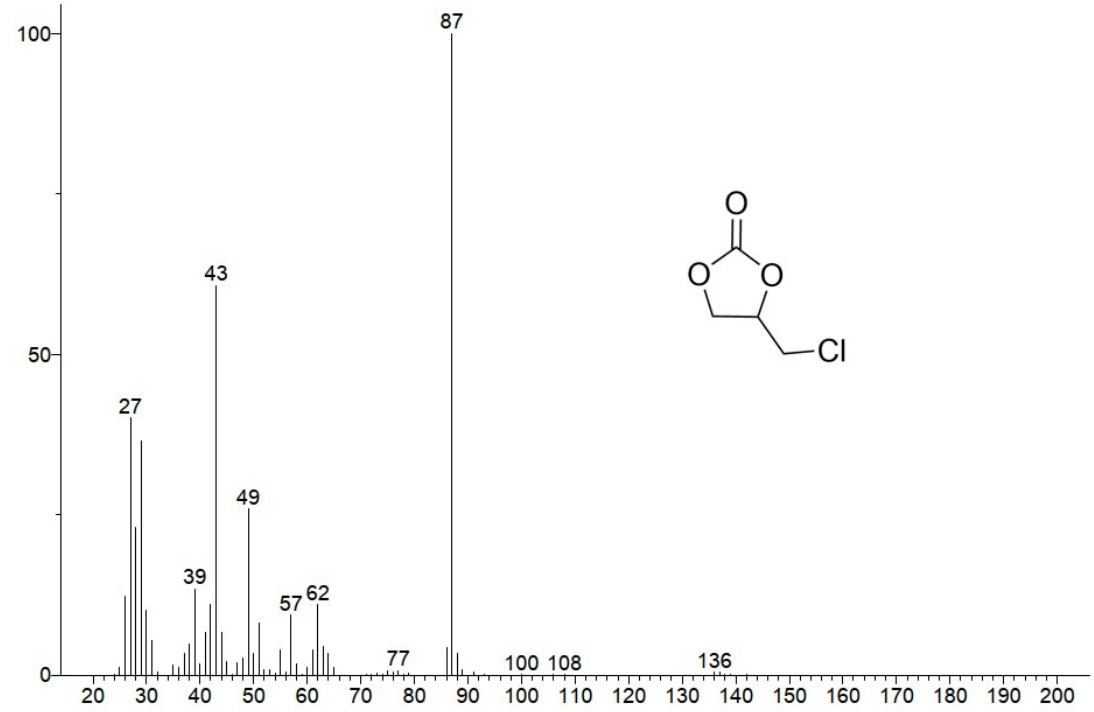


(Text File) E62#1010 RT: 3.50 AV: 1

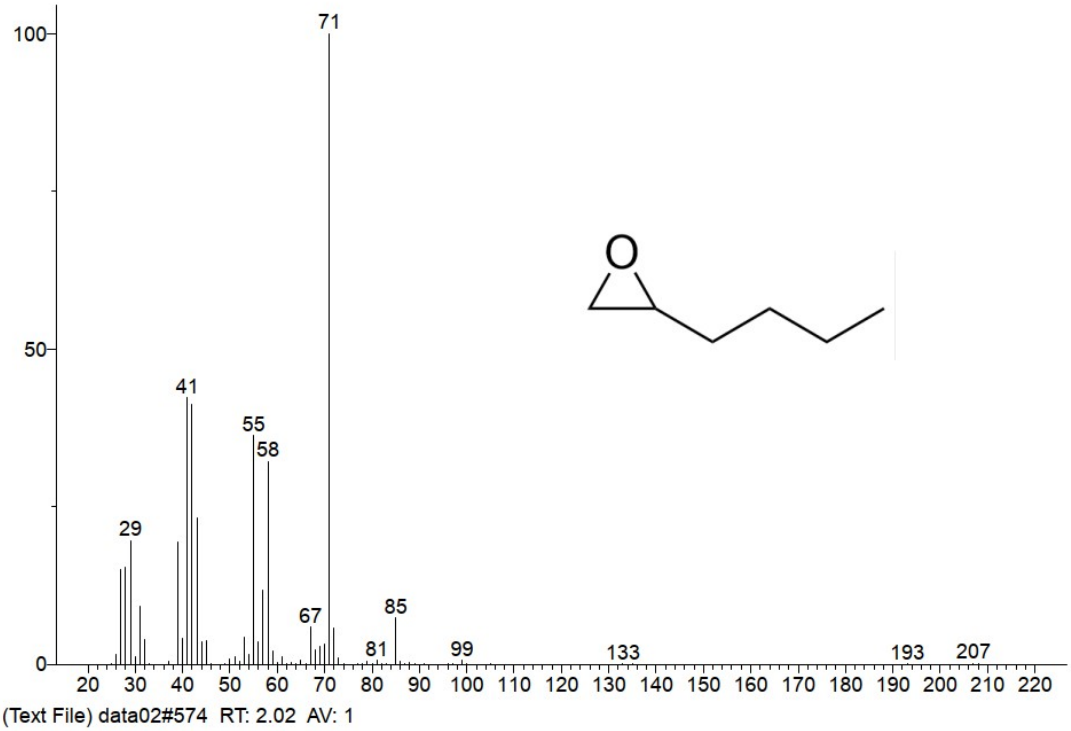


(Text File) data02#574 RT: 2.02 AV: 1

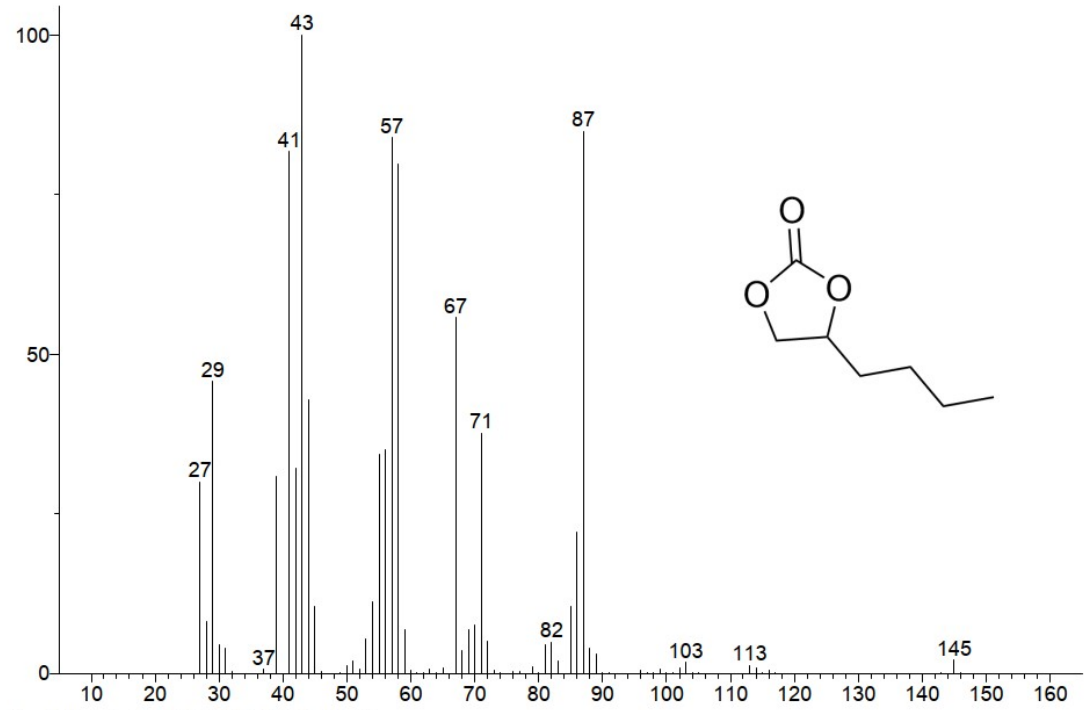


(Text File) data01#2153 RT: 7.39 AV: 1

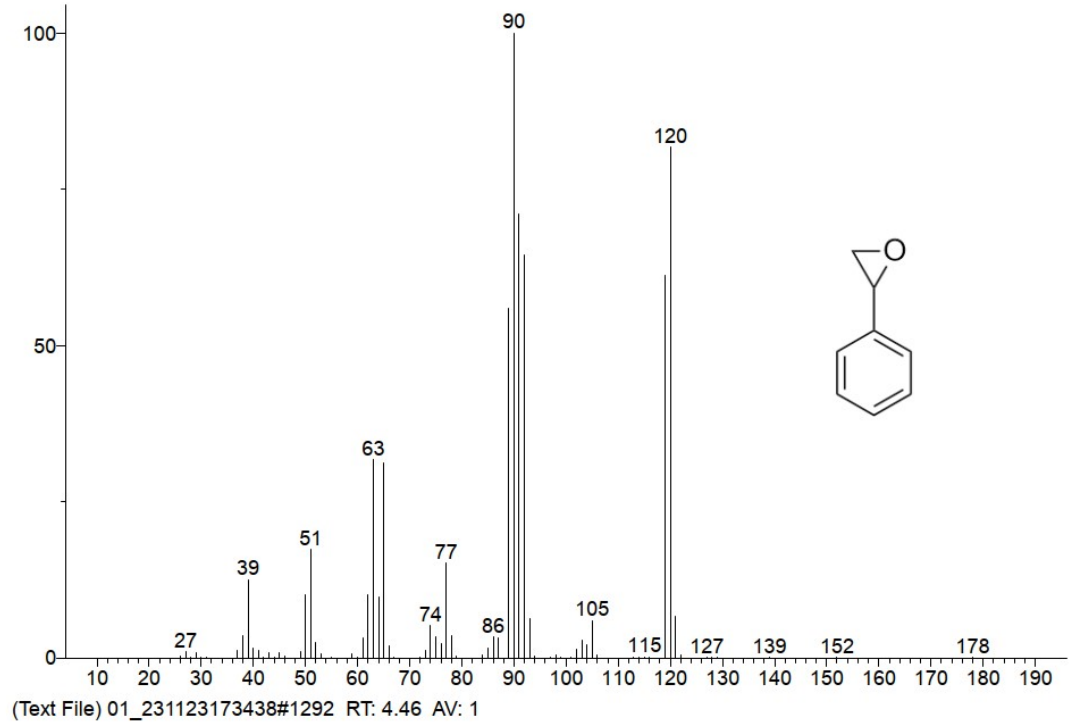


(Text File) 01_231123173438#1292 RT: 4.46 AV: 1

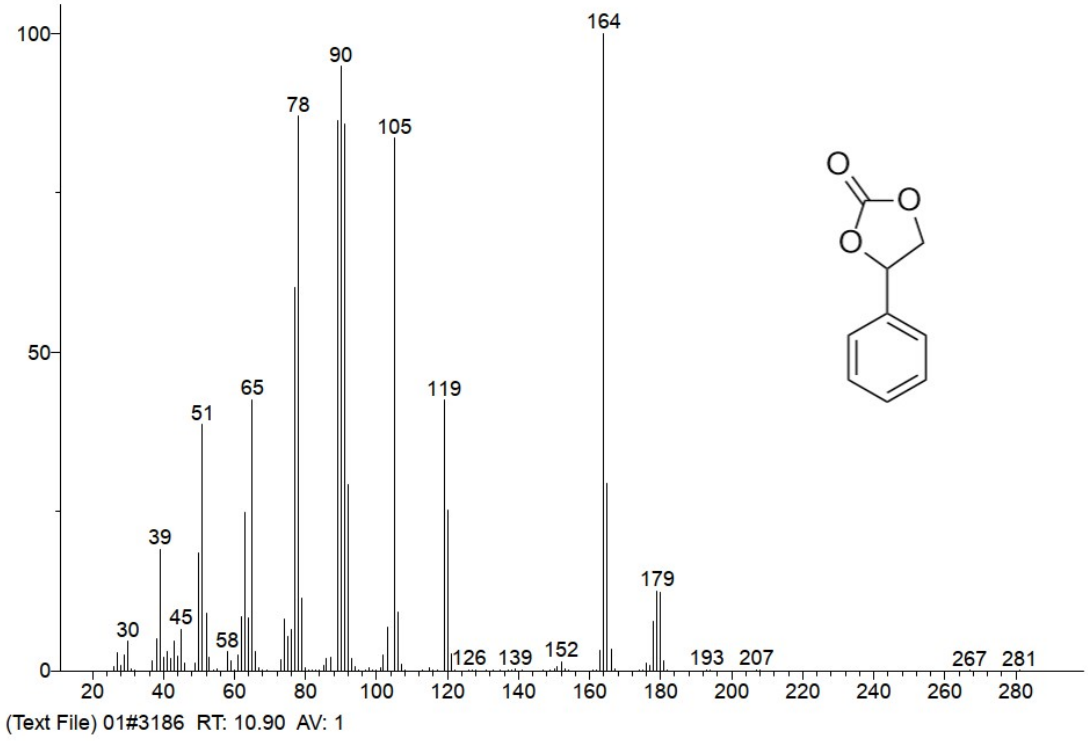


(Text File) 01#3186 RT: 10.90 AV: 1

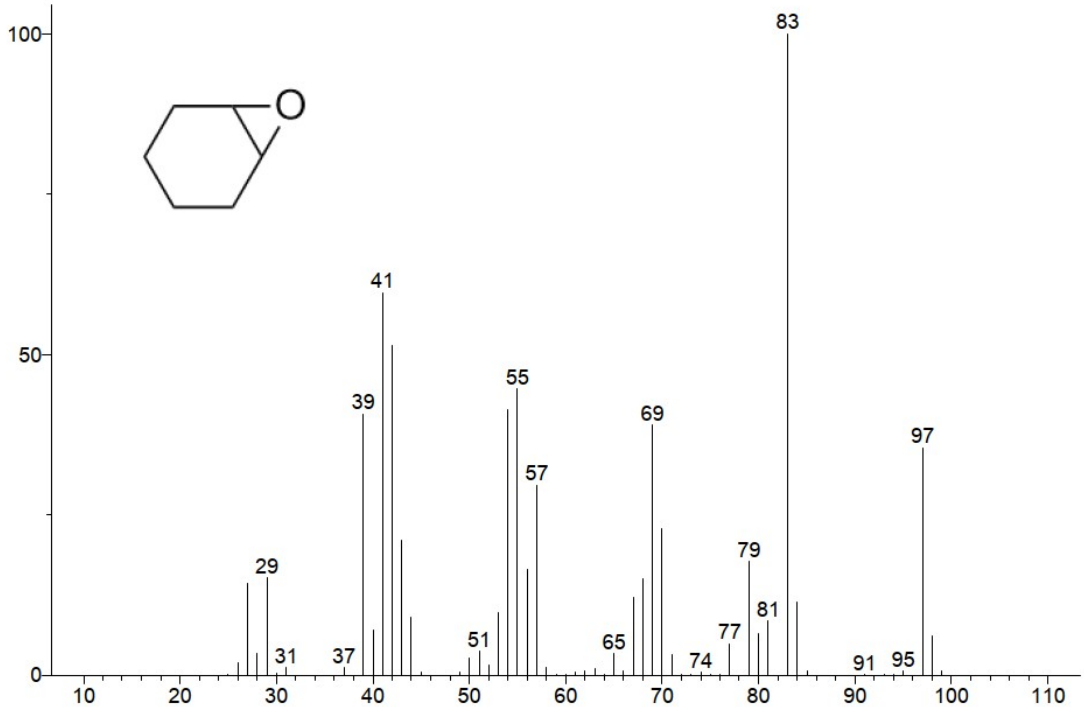


(Text File) 02#699 RT: 2.44 AV: 1

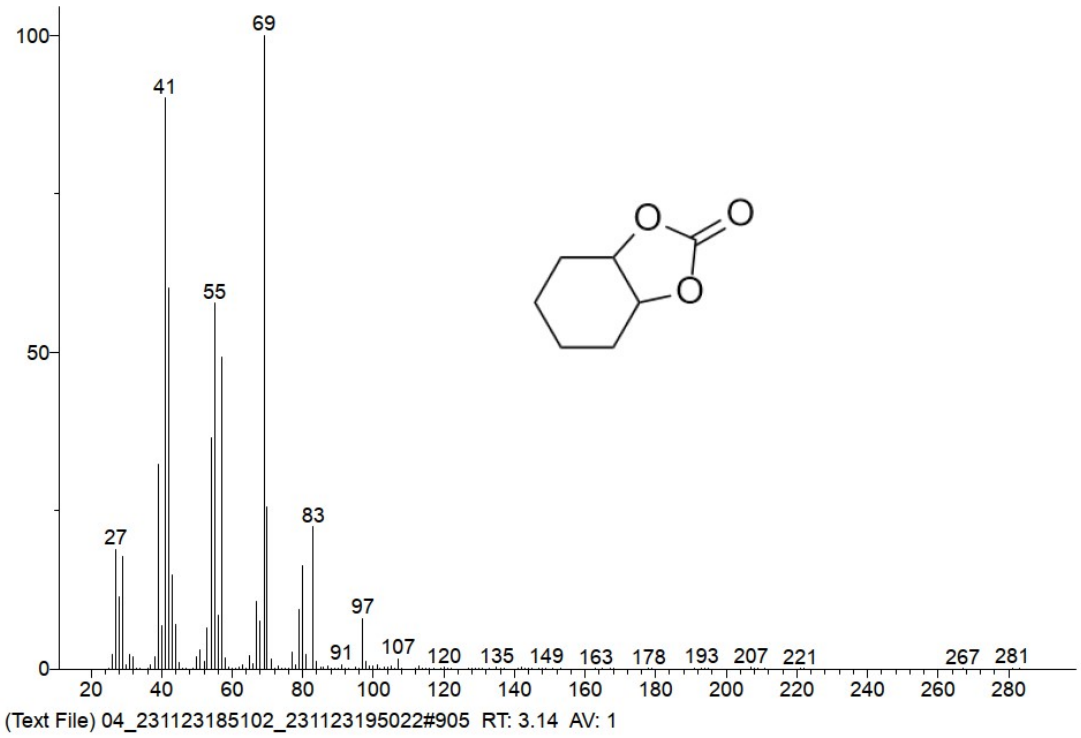


**Reference**

(1) Shearer; Greig; Chavan; Sachin; Bordiga; Silvia; Svelle; Stian; Olsbye., Defect Engineering: Tuning the Porosity and Composition of the Metal-Organic Framework UiO-66 via Modulated Synthesis. *Chemistry of Materials* **2016**, *28*, 3749-3761.

(2) Valenzano, L.; Civalleri, B.; Chavan, S.; Bordiga, S.; Nilsen, M. H.; Jakobsen, S., Disclosing the complex structure of UiO-66 metal organic framework: a synergic combination of experiment and theory. *Chemistry of Materials*, **2011**, *23*, 1700-1718.

(3) Hattenhauer; Karen; Kerton; Francesca; M.; Collins; Julie; Alhashmialameer; Dalal., Iron Amino-bis(phenolate) Complexes for the Formation of Organic Carbonates from $CO_2$ and Oxiranes. *Catalysis science & technology*. **2016**, *6*, 5364-5373.

(4) Chen, Y.; Yu, J.; Yang, Y.; Huo, F.; Li, C., A Continuous Process for Cyclic Carbonate Synthesis from $CO_2$ Catalyzed by the Ionic Liquid in a Microreactor

System: Reaction Kinetics, Mass Transfer, and Process Optimization. *Chemical Engineering Journal* **2023**, *455*, 140670.

(5) Daeho; Kim; Kyungsu., Organic-Inorganic Multifunctional Hybrid Catalyst Giving Catalytic Synergies in Cooperative Coupling between $CO_2$ and Propylene Oxide to Propylene Carbonate. *Journal of $CO_2$ Utilization* **2018**, *27*, 129-136.

(6) Liu, M.; Liu, B.; Zhong, S.; Shi, L.; Sun, J., Kinetics and Mechanistic Insight into Efficient Fixation of $CO_2$ to Epoxides over N-Heterocyclic Compound/$ZnBr_2$ Catalysts. *Industrial & Engineering Chemistry Research* **2015**, *54*, 633-640.

(7) Li, Q.; Dai, W.; Mao, J., Facile Integration of Hydroxyl Ionic Liquid into Cr-MIL-101 as Multifunctional Heterogeneous Catalyst for Promoting the Efficiency of $CO_2$ Conversion. *Microporous and Mesoporous Materials* **2023**, *350*, 112461.

(8) Babu, R.; Kathalikkattil, A. C.; Roshan, R.; Tharun, J.; Kim, D.-W.; Park, D.-W., Dual-porous metal organic framework for room temperature $CO_2$ fixation via cyclic carbonate synthesis. *Green Chemistry* **2016**, *18*, 232-242.

(9) Khan, S.; Sama, F.; Alfuhaid, L. T.; Hoque, B.; Helal, A., Harnessing the Utility of Mechanochemically Synthesized 2D Imine-Linked Covalent Organic Framework Doped with Nickel Nanoparticles for Solvent-Free $CO_2$ Conversion at Atmospheric Pressure. *ACS Appl. Nano Mater.* **2025**, *8*, 15834-15849.

(10) Ding, M.; Jiang, H. L., Incorporation of Imidazolium-Based Poly(ionic liquid)s into a Metal-Organic Framework for $CO_2$ Capture and Conversion. *ACS Catalysis* **2018**, *8*, 3194-3201.

(11) Kurisingal, J. F.; Rachuri, Y.; Pillai, R. S.; Gu, Y.; Choe, Y.; Park, D.-W., Ionic-Liquid-Functionalized UiO-66 Framework: An Experimental and Theoretical Study on the Cycloaddition of $CO_2$ and Epoxides. *ChemSusChem* **2019**, *12*, 1033-1042.

(12) Liu, D.; Li, G.; Liu, H., Functionalized MIL-101 with imidazolium-based ionic liquids for the cycloaddition of $CO_2$ and epoxides under mild condition. *Appl. Surf. Sci*. **2018**, *428*, 218-225.